Supplementary Information

Significantly improved breakdown strength and energy density in high-temperature polymer dielectric enabled by bilayered nanocoatings

Chuchu Guo,[a] Honglin Guo,[b] Peilin Yang,[b] Yan-Jun Liu,[c] Zhengshi Chang,*[b] Jie Chen,*[d] Bin Yao,[e] Jierui Zhou,[f] and Yifei Wang*[a]

[a] *State Key Laboratory for Mechanical Behavior of Materials, School of Materials Science and Engineering, Xi'an Jiaotong University, Xi'an, 710049, China*
E-mail: yifei.wang@xjtu.edu.cn
[b] *State Key Laboratory of Electrical Insulation and Power Equipment, School of Electrical Engineering, Xi'an Jiaotong University, Xi'an, 710049, China*
Email: changzhsh1984@163.com
[c] *School of Science, Lanzhou University of Technology, Lanzhou 730050, China*
[d] *Shaanxi Key Laboratory of Optoelectronic Functional Materials and Devices, School of Materials Science and Chemical Engineering, Xi'an Technological University, Xi'an 710032, China*
Email: chenjie@xatu.edu.cn
[e] *School of Aerospace Science and Technology, Xidian University, Xi'an 710071, China*
[f] *Electrical Insulation Research Center, Institute of Materials Science, University of Connecticut, Storrs, CT 06269, USA*

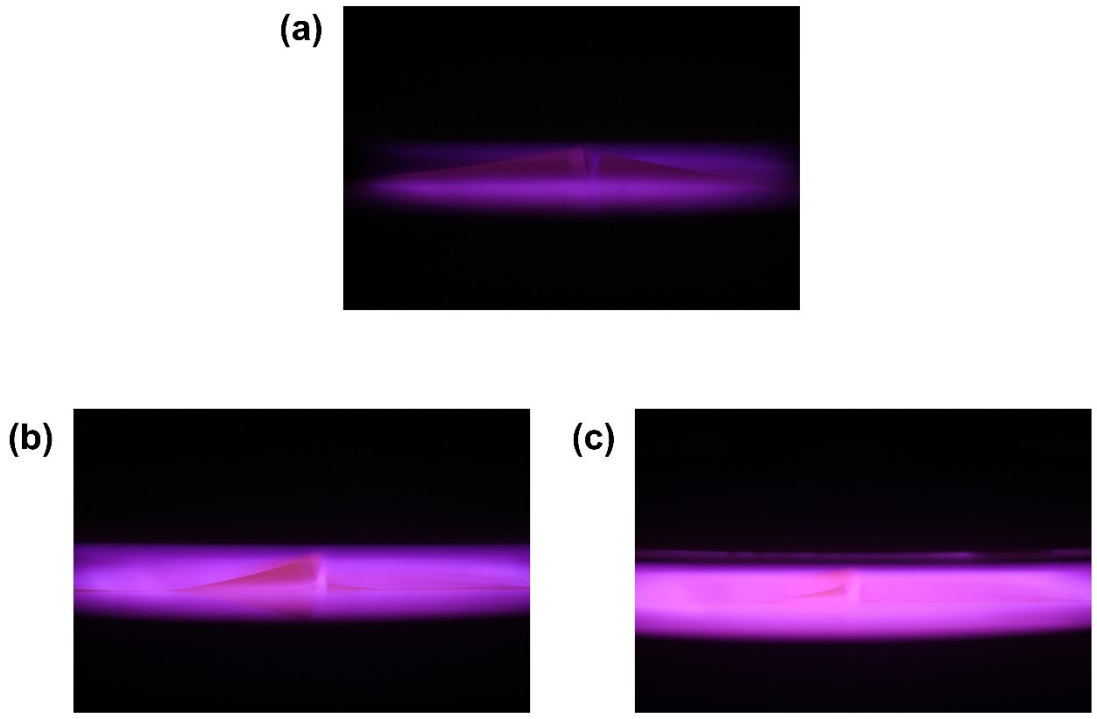

Fig. S1. Plasma discharge images in He/Air (4:1) mixture at different applied voltages: (a) 1.2 kV, (b) 2.2 kV, and (c) 3.2 kV

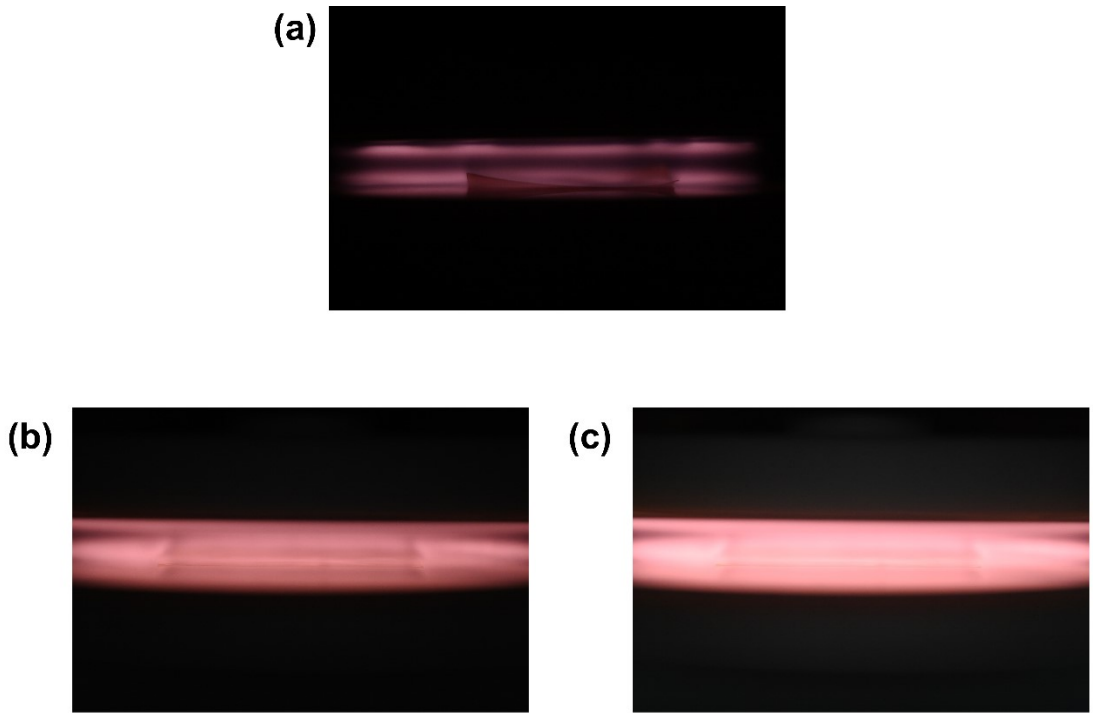

Fig. S2. Plasma discharge images in He/O_2 (4:1) mixture at different applied voltages: (a) 1.4 kV, (b) 2.5 kV, and (c) 3.6 kV

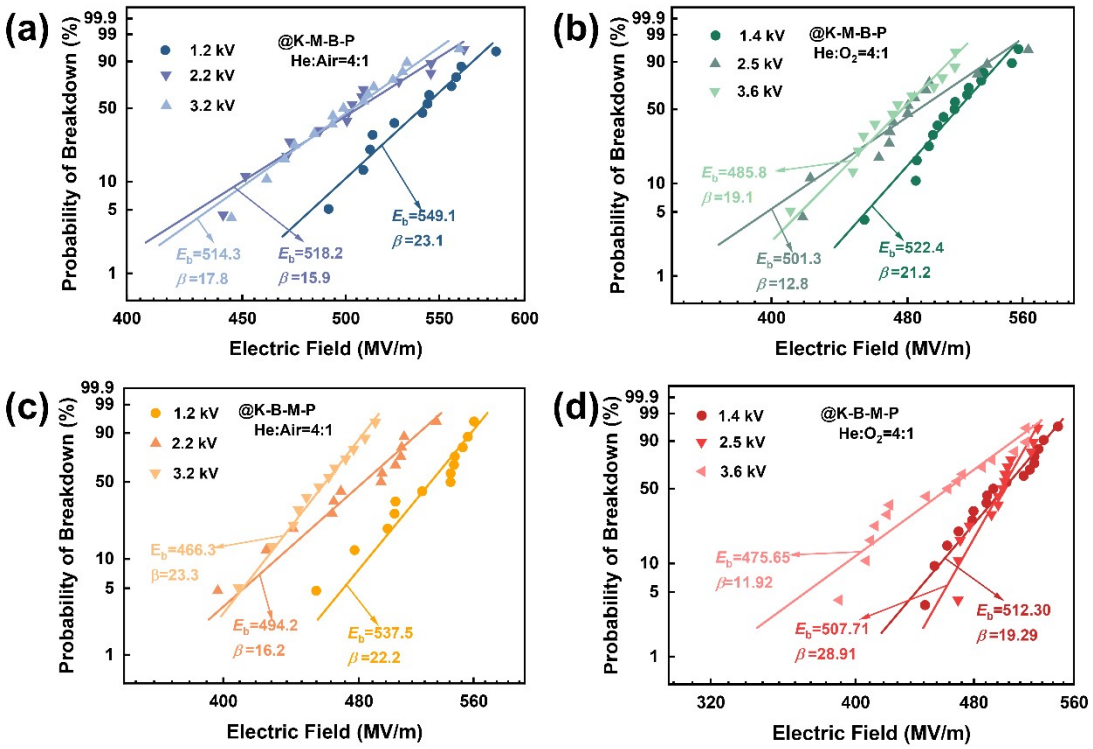

Fig. S3. Weibull distributions of K–M–B–P and K–B–M–P samples treated with different discharge voltages and plasma atmospheres at room temperature.

The effects of discharge voltage and plasma atmosphere on the breakdown performance were systematically investigated at room temperature and a fixed pressure of 2.0 kPa. As shown in Fig. S3, the breakdown strength of the samples exhibits an overall decreasing trend with increasing discharge voltage, suggesting that excessively intense plasma treatment may adversely affect the stability of the interfacial structure. Additionally, the plasma atmosphere significantly influences the breakdown performance. Samples treated in a He/air mixture consistently outperform those treated in a He/O_2 atmosphere, indicating that the composition of active species in the plasma plays a crucial role in interfacial modification. Notably, under the optimal plasma treatment conditions of He/air (volume ratio 4:1) at a discharge voltage of 1.2 kV, the

K–M–B–P sample achieves the highest breakdown performance, with an E_b of 549.1 MV m^{-1} and a β of 23.1.

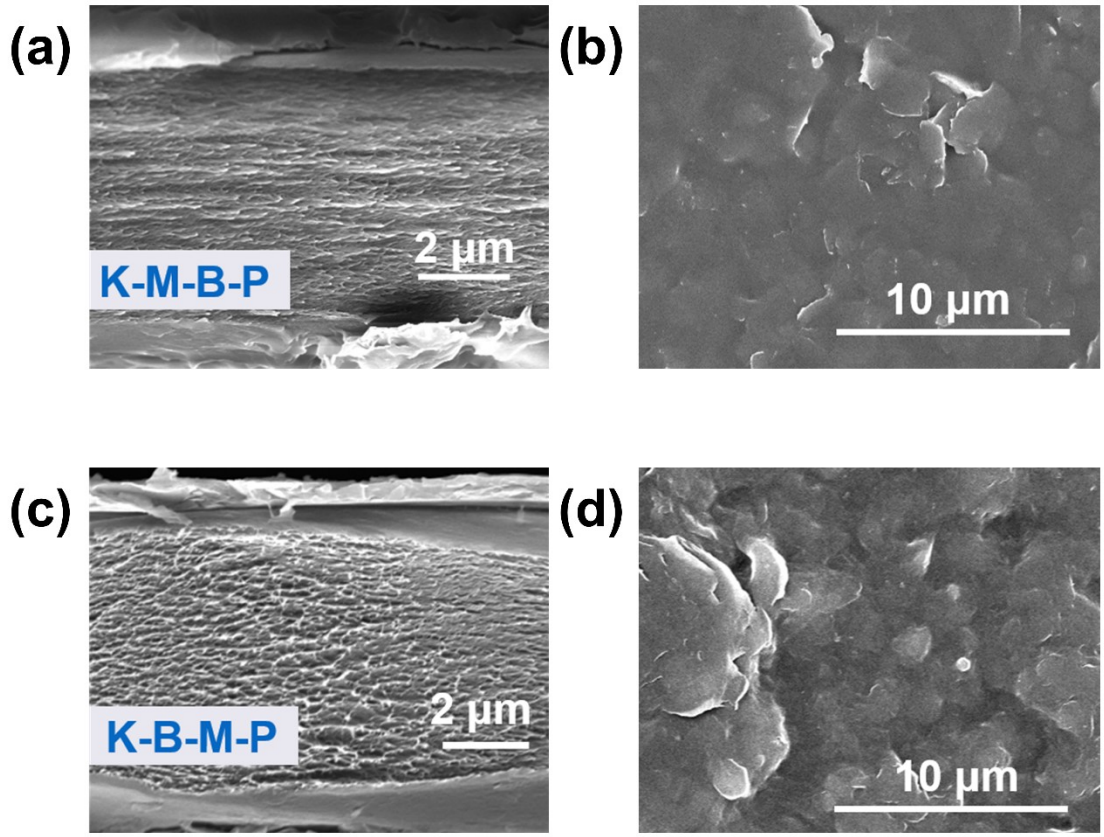

Fig. S4. SEM images of (a) cross-section and (b) surface of K–M–B–P; (c) cross-section and (d) surface of K–B–M–P.

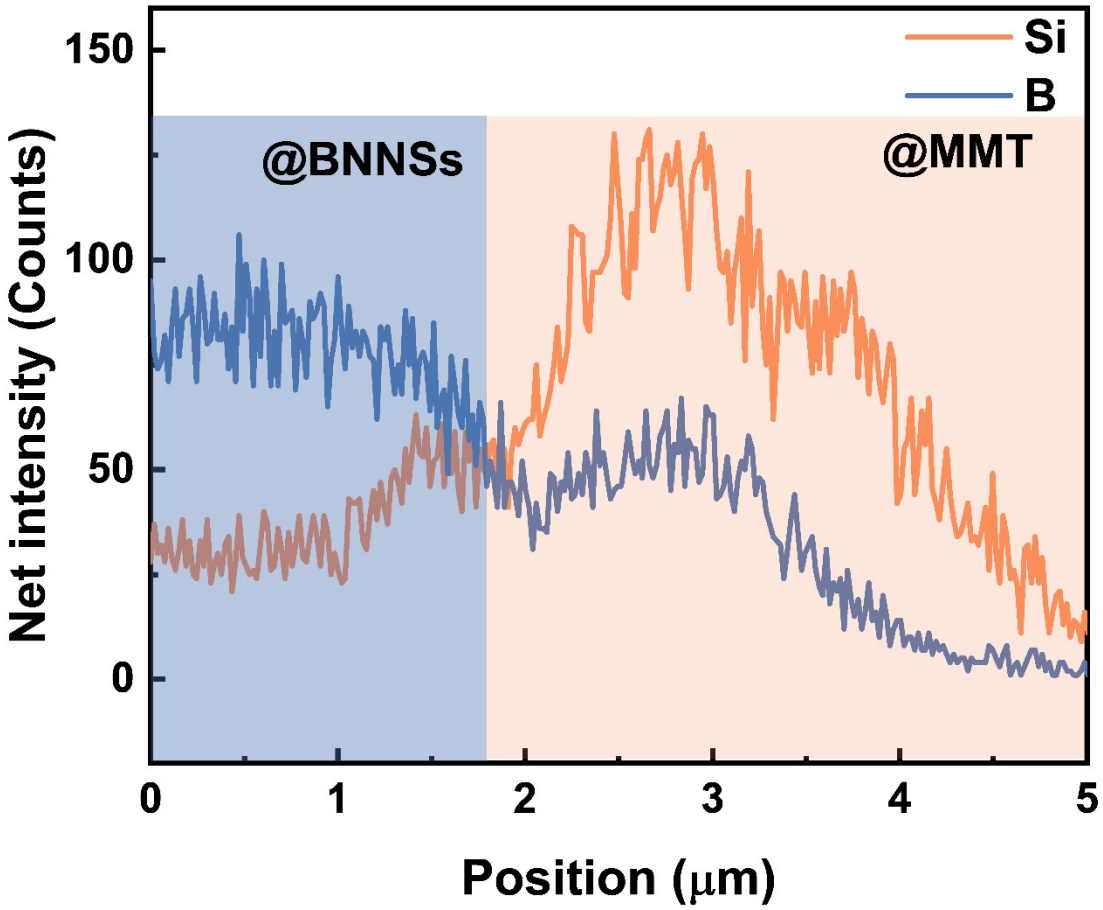

Fig. S5. EDS line scan profiles of the K–B–M–P sample.

The cross-sectional and surface SEM images of the K–B–M–P sample, together with the corresponding EDS line-scan profiles, are provided in Figs. S4c, S4d, and S5. Similar to the K–M–B–P sample, a structurally intact bilayer nanocoating is formed, featuring continuous interfaces and tight interlayer adhesion.

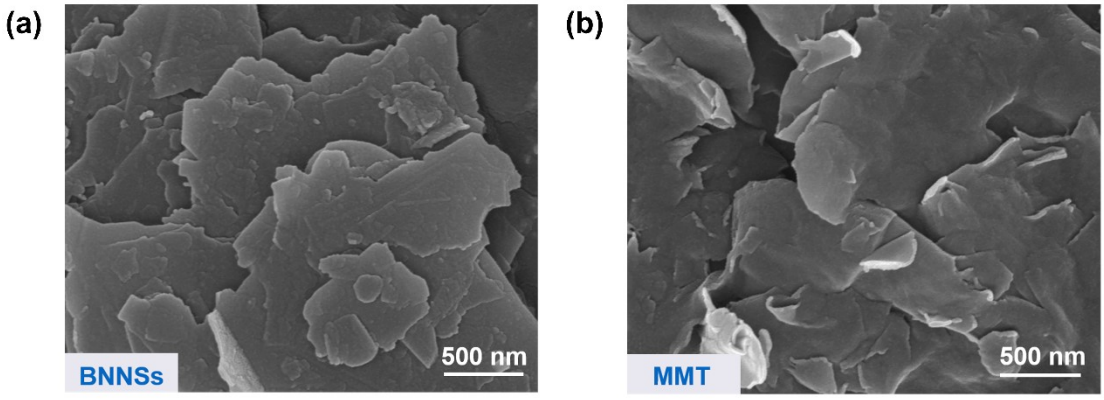

Fig. S6. SEM images of (a) BNNSs and (b) MMT nanosheets.

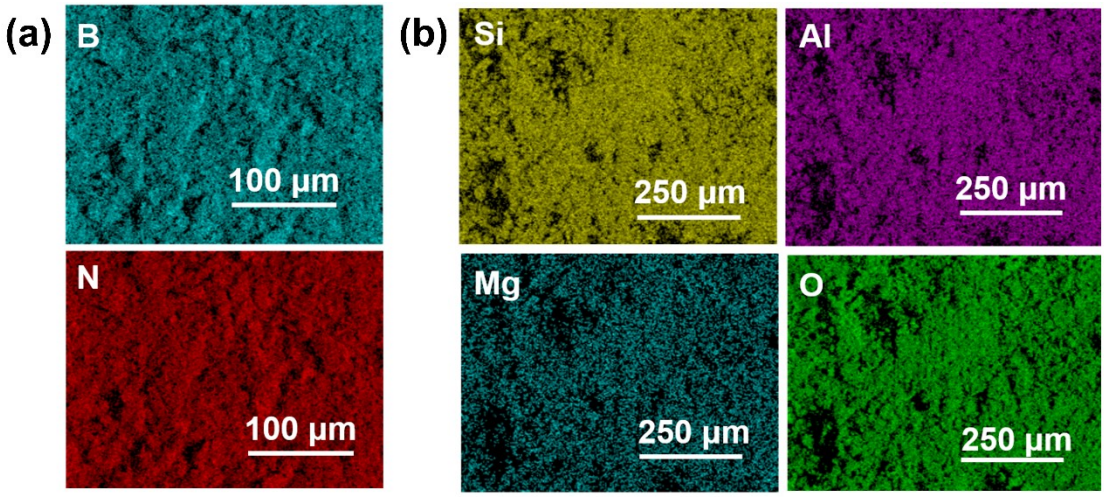

Fig. S7. EDS mapping images of (a) BNNSs and (b) MMT nanosheets.

The corresponding EDS elemental mapping results (Fig. S7) reveal a uniform distribution of B and N elements within the BNNSs, while Si, Al, O, and Mg elements are homogeneously distributed throughout the MMT nanosheets, indicating good compositional homogeneity.

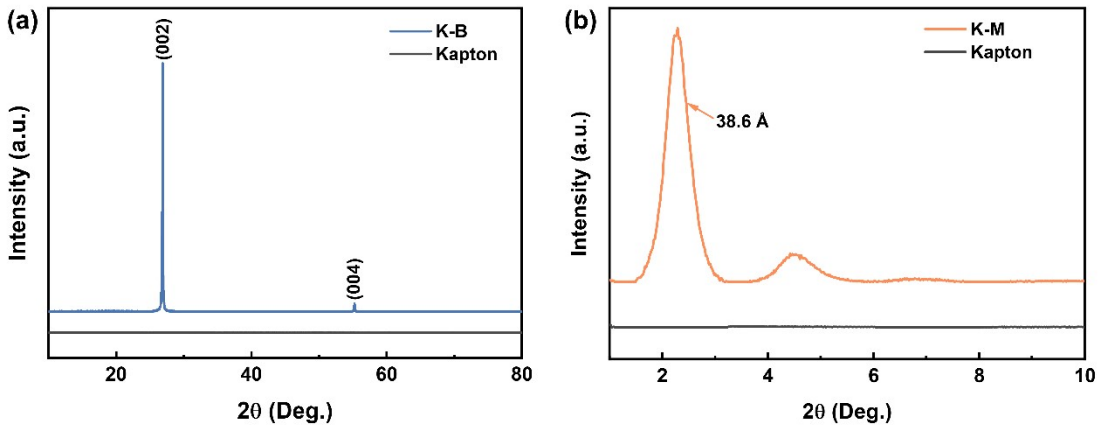

Fig. S8. XRD patterns of the Kapton PI film compared with (a) K–B and (b) K–M samples.

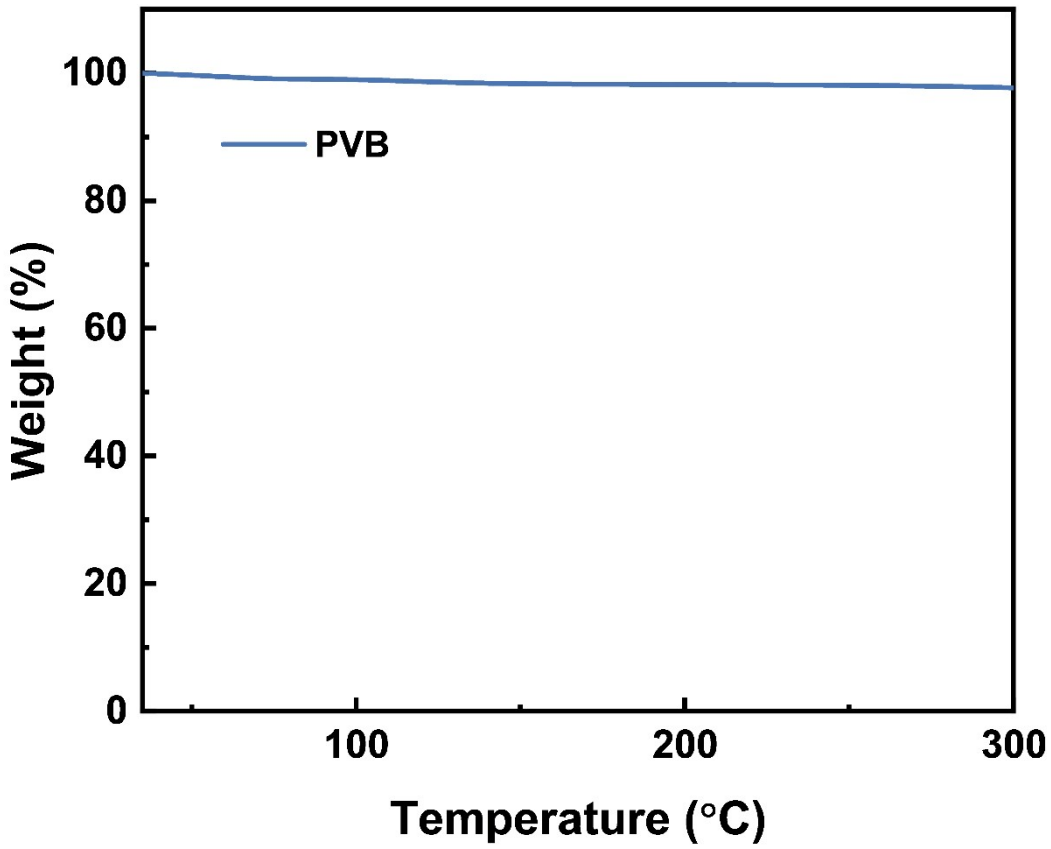

Fig. S9. TGA curve of PVB measured from room temperature to 300 °C.

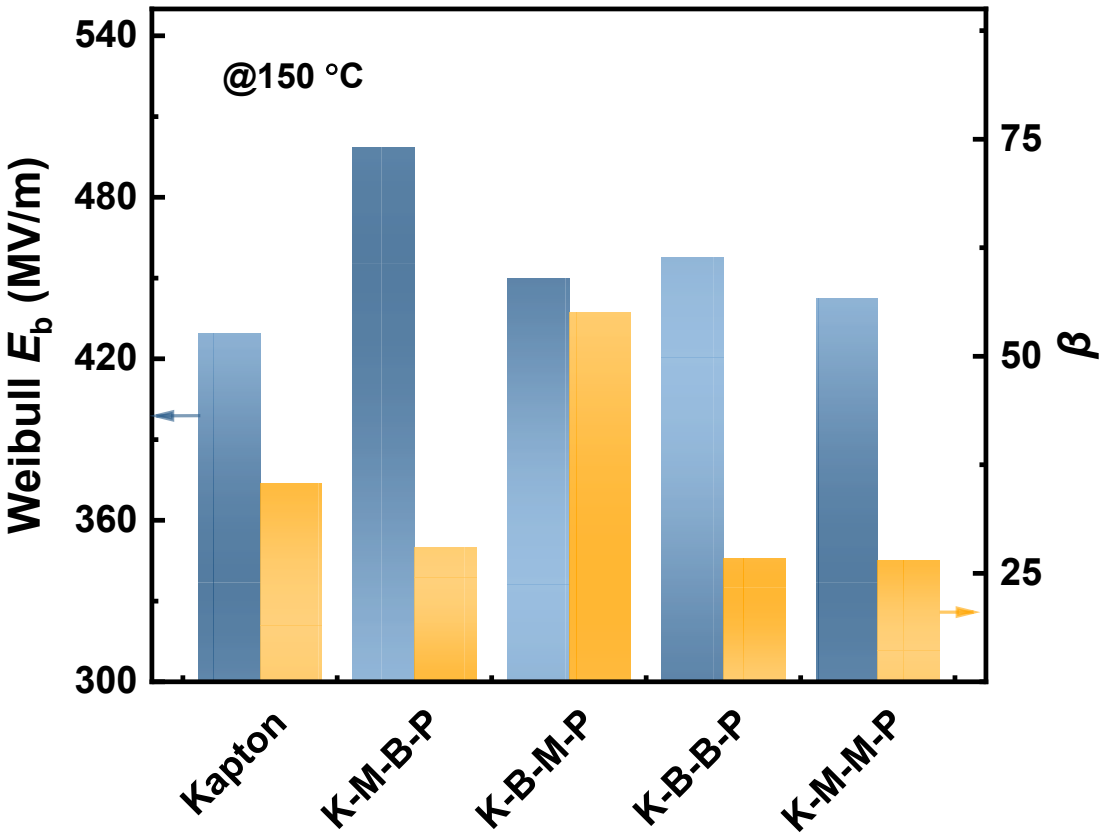

Fig. S10. *E*b and β of different bilayer nanocoated Kapton PI films at 150 °C.

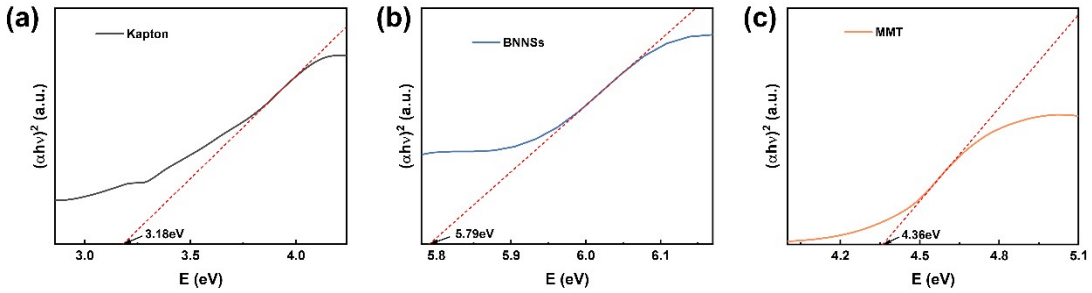

Fig. S11. Optical bandgaps of (a) Kapton PI film, (b) BNNSs, and (c) MMT nanosheets determined from UV-vis spectra.

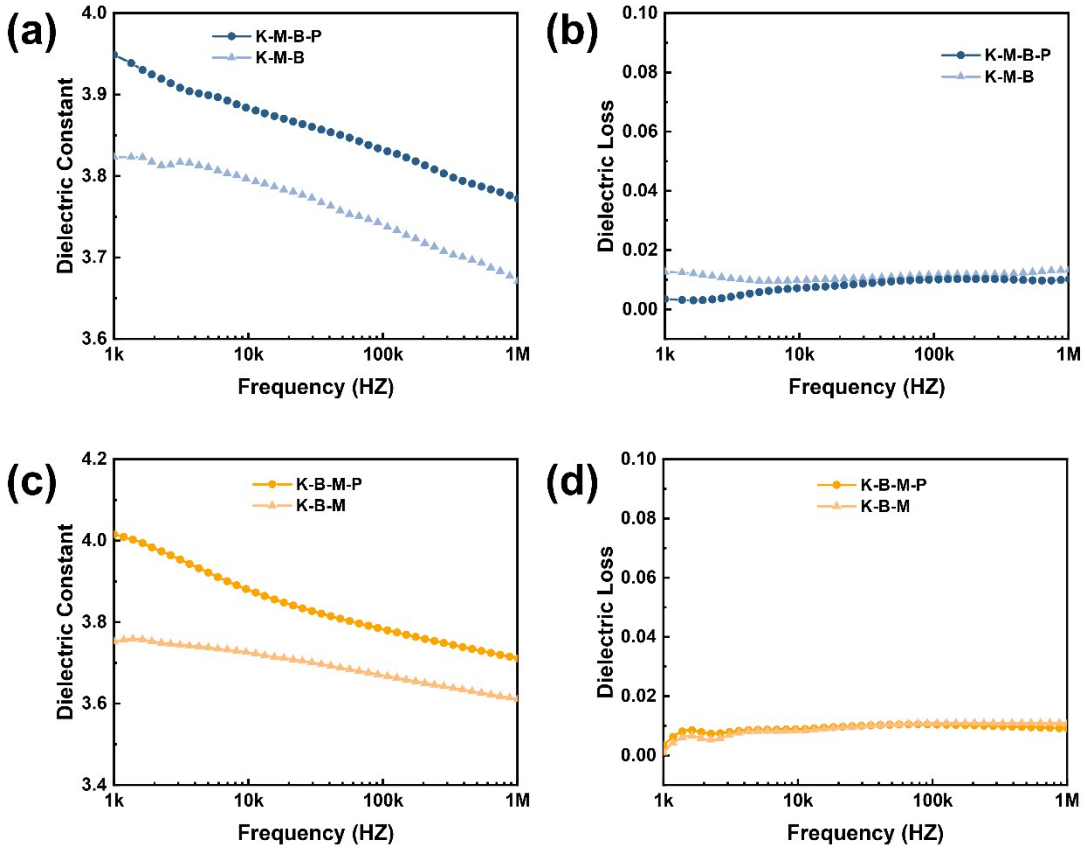

Fig. S12. Dielectric properties of different film configurations: ϵr and tanδ for (a, b) K–M–B–P and K–M–B, and (c, d) K–B–M–P and K–B–M.

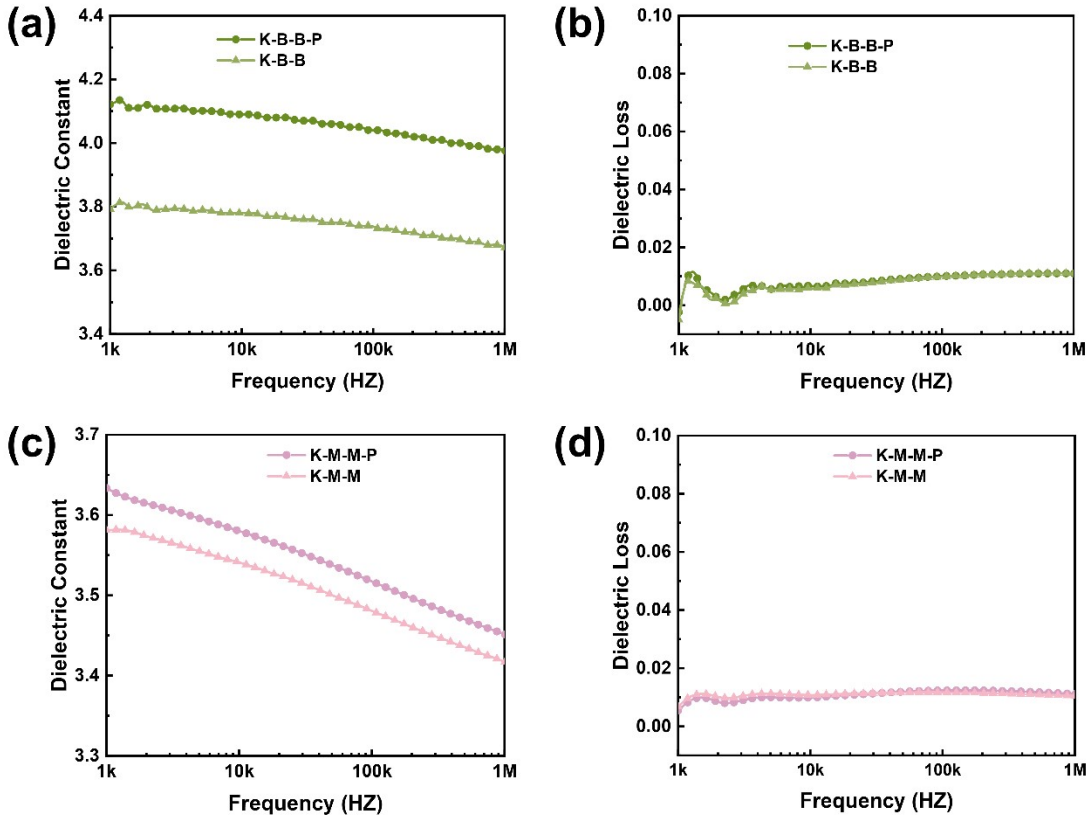

Fig. S13. Dielectric properties of different film configurations: ϵ_r and tanδ for (a, b) K–B–B–P and K–B–B, and (c, d) K–M–M–P and K–M–M.

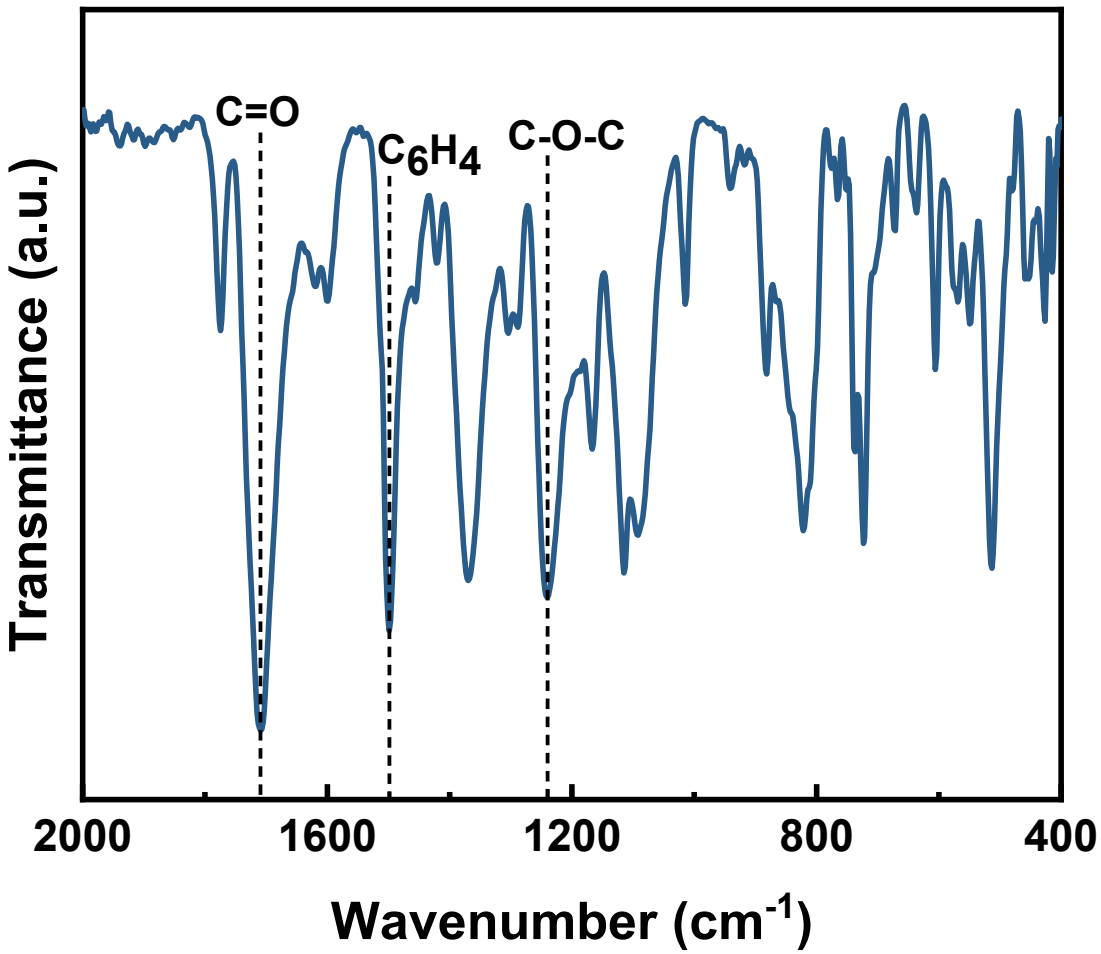

Fig.S14. FTIR difference spectrum of Kapton PI film (plasma-treated-–pristine).

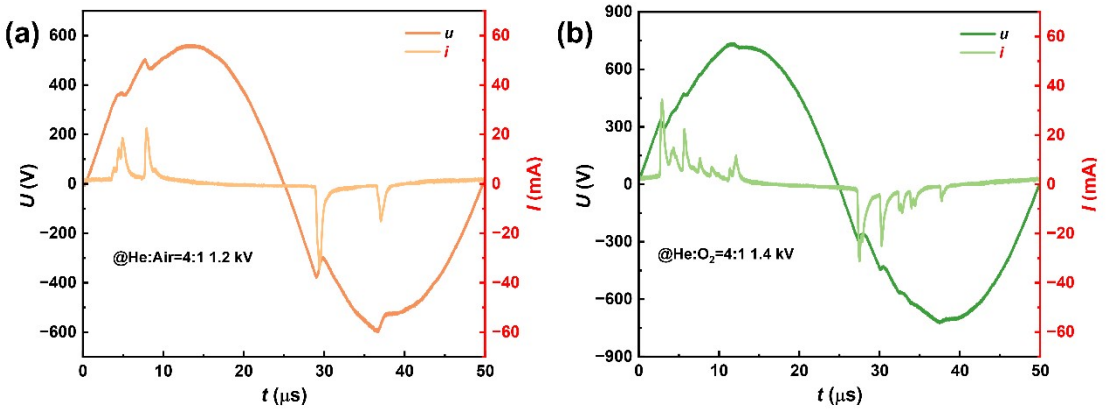

Fig.S15. Voltage–current (V–I) waveforms of the plasma discharge in different gas atmospheres: (a) He/Air and (b) He/O_2.

The voltage–current waveforms and discharge images of the plasma are shown in Figs. S1, S2, and S14. Within one complete AC voltage cycle, the dielectric barrier discharge (DBD) process exhibits two primary discharge periods, occurring shortly after the zero-crossing points in the positive and negative half-cycles, respectively. Each discharge period consists of an initial dominant discharge peak followed by several secondary discharge peaks. Under the same He volume fraction, the discharge inception voltage in the He/air mixture is 1.2 kV, slightly lower than that in the He/O_2 atmosphere (1.4 kV). Meanwhile, the duration of each discharge period in the He/air mixture is significantly prolonged, with a noticeable reduction in the number of discharge events, indicating a longer sustained plasma discharge. Correspondingly, the discharge images reveal typical glow discharge characteristics in both atmospheres; however, the overall discharge intensity in the He/air environment is markedly higher than that in the He/O_2 atmosphere. In terms of emission color, the dominant emission lines from He and O atoms are concentrated in the 550–850 nm wavelength range, resulting in an orange-red plasma appearance in the He/O_2 atmosphere. In contrast, the emission bands from nitrogen-containing active species such as N_2 and N_2^+ are primarily located in the ultraviolet region (300–400 nm), giving rise to a distinct purple glow characteristic of the plasma in the He/air atmosphere.

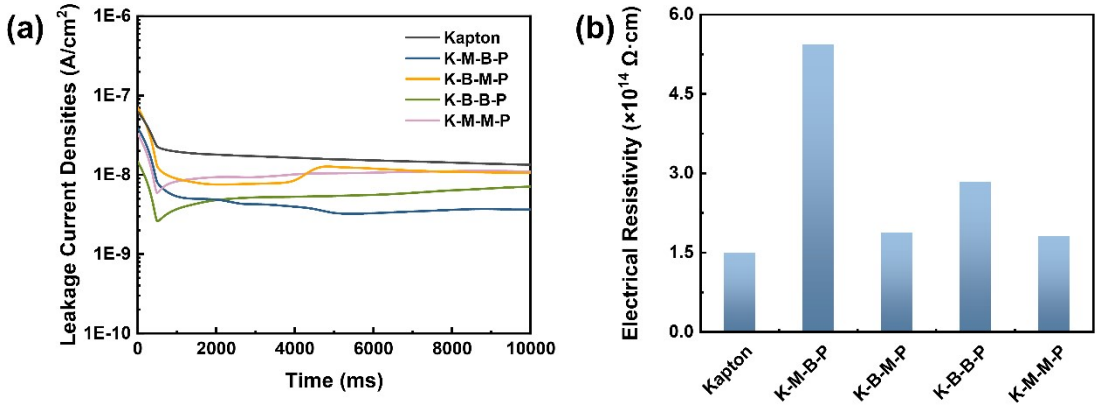

Fig. S16. Leakage current and electrical resistivity of bilayer nanocoated Kapton PI films and pristine Kapton PI measured at room temperature under an electric field of

200 MV m^{-1}. (a) Leakage current density as a function of time. (b) Comparison of the electrical resistivity of the corresponding films.

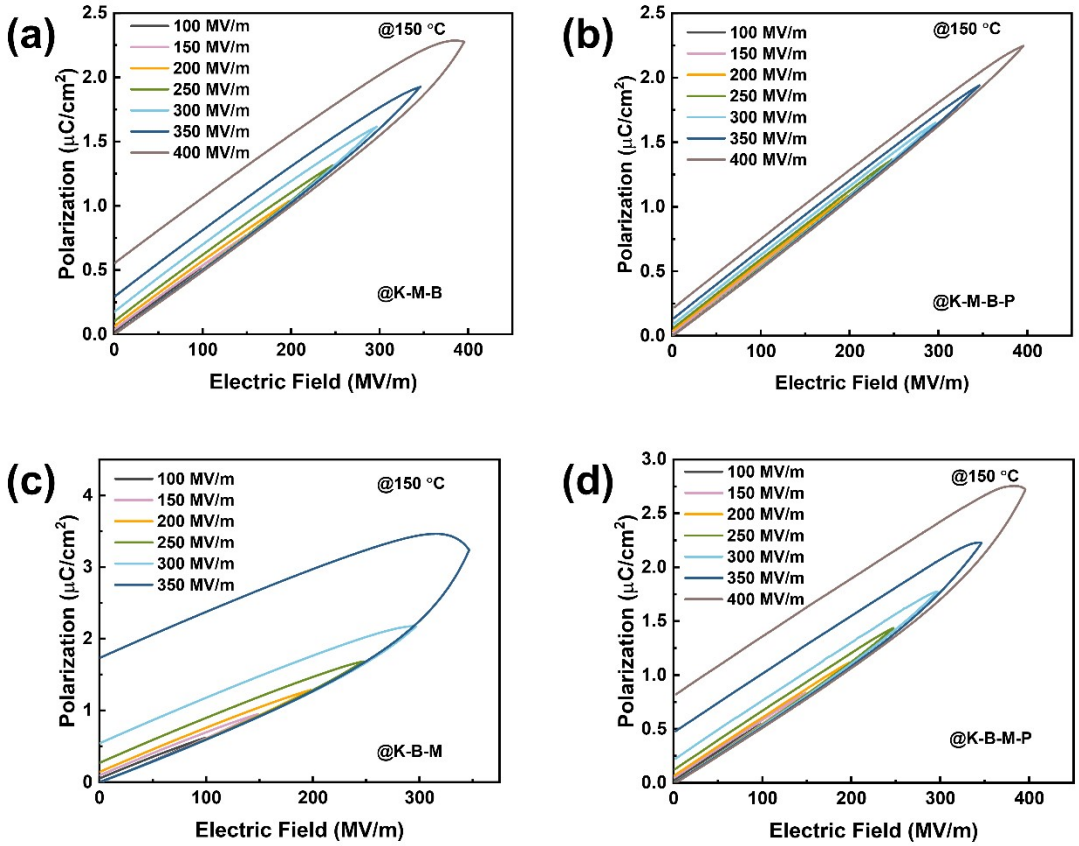

Fig. S17. *P*–*E* hysteresis loops of (a) K–M–B, (b) K–M–B–P, (c) K–B–M, and (d) K–B–M–P measured at 150 °C.

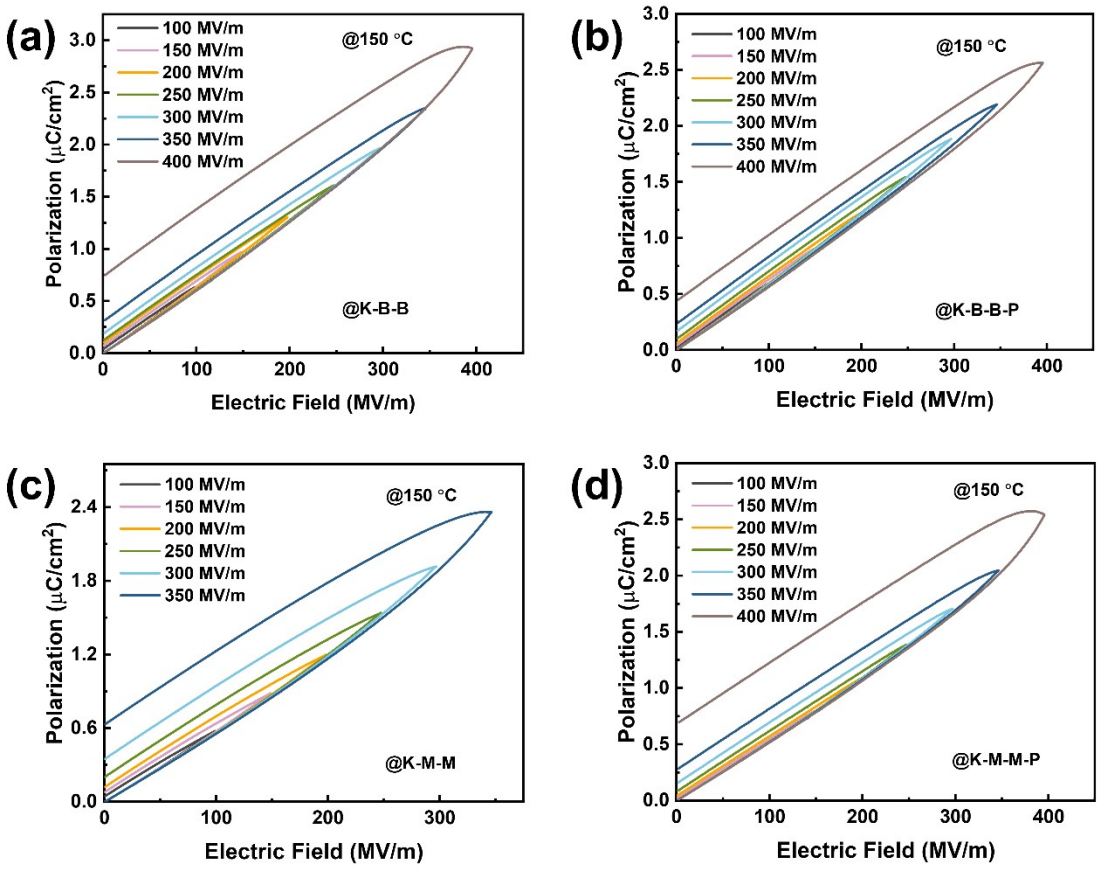

Fig. S18. *P–E* hysteresis loops of (a) K–B–B, (b) K–B–B–P, (c) K–M–M, and (d) K–M–M–P measured at 150 °C.

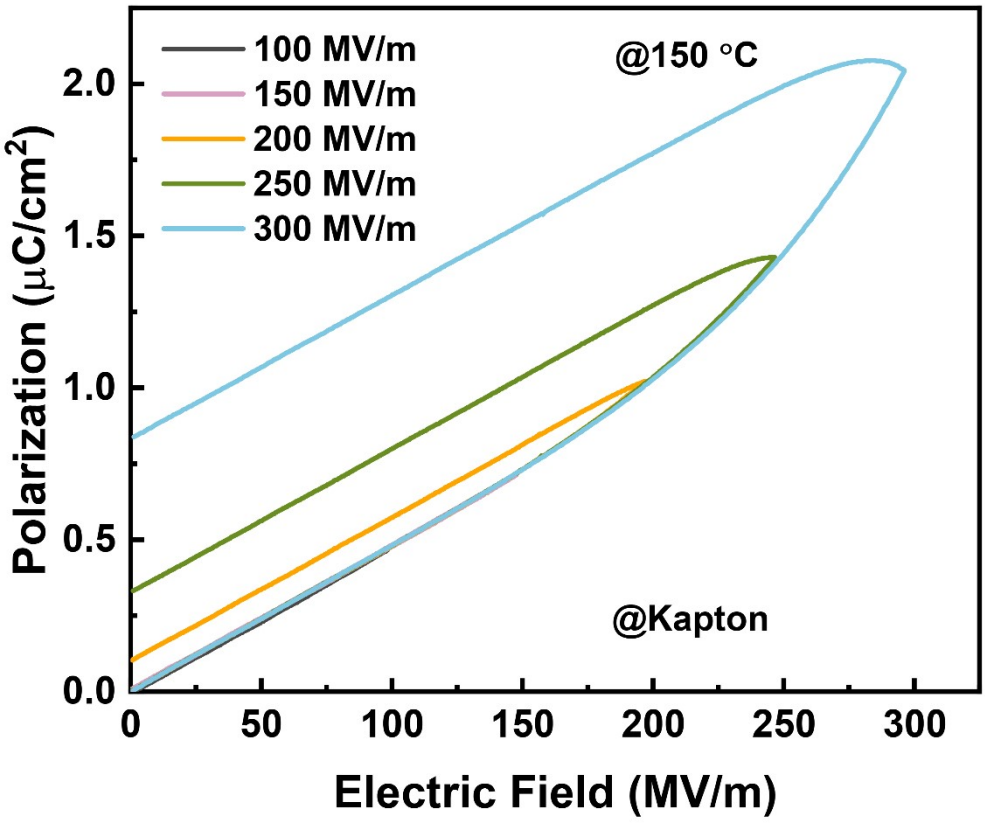

Fig. S19. *P–E* hysteresis loops of the pristine Kapton PI film measured at 150 °C.

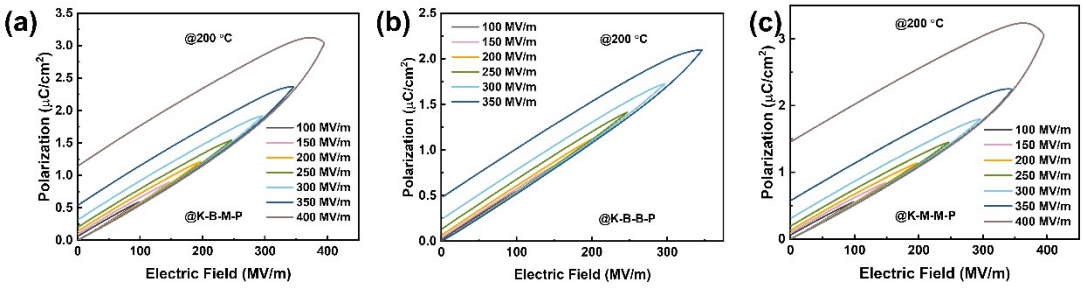

Fig. S20. *P–E* hysteresis loops of (a) K–B–M–P, (b) K–B–B–P and (d) K–M–M–P measured at 200 °C.

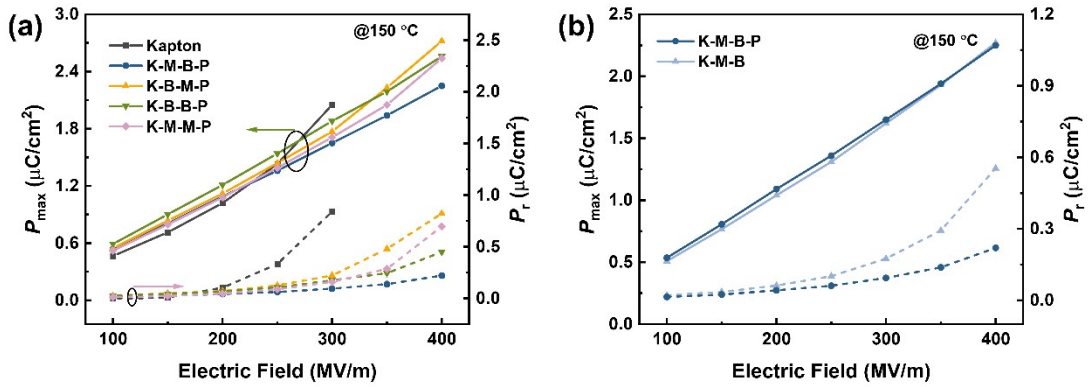

Fig. S21. Polarization performance at 150 °C: (a) P_{max} and P_r of the bilayer nanocoated PI films; (b) Comparison of P_{max} and P_r between the K–M–B–P and K–M–B samples.

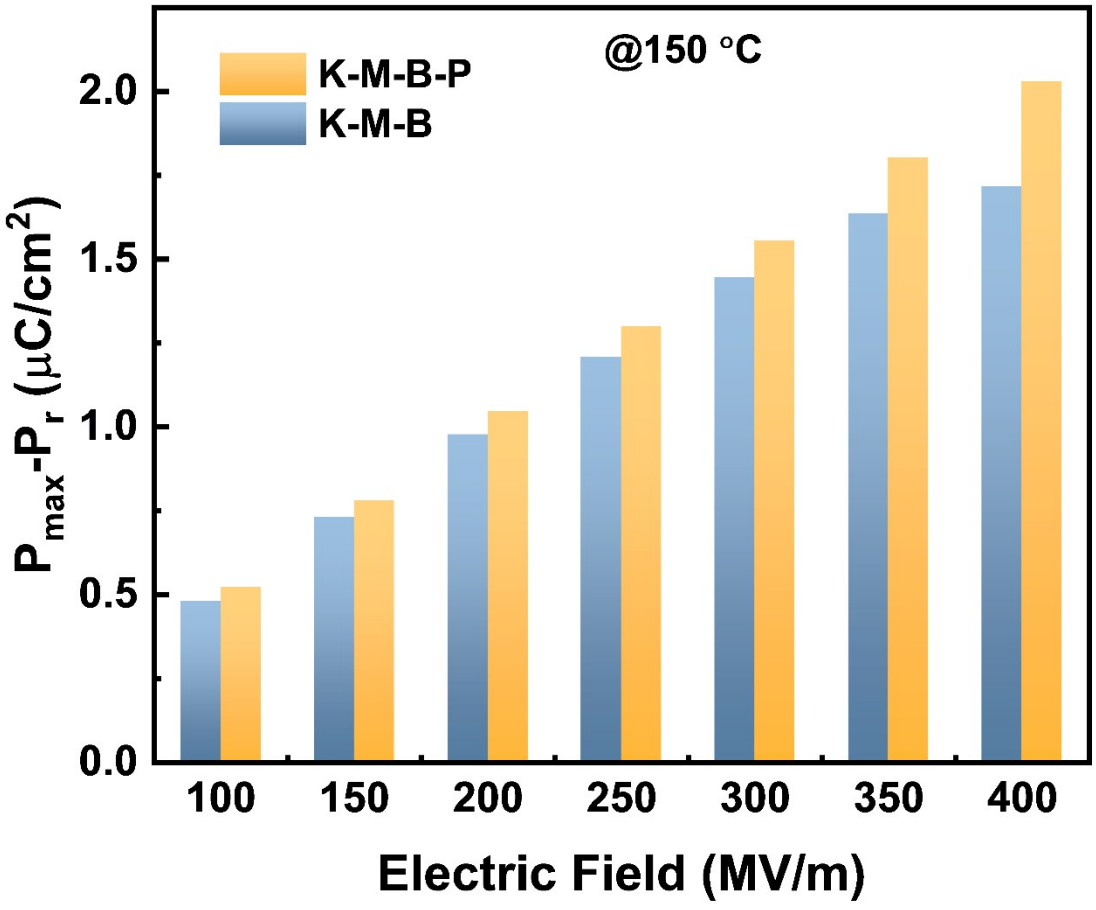

Fig. S22. Electric field dependence of $P_{max} - P_r$ for the K–M–B and K–M–B–P samples measured at 150 °C.

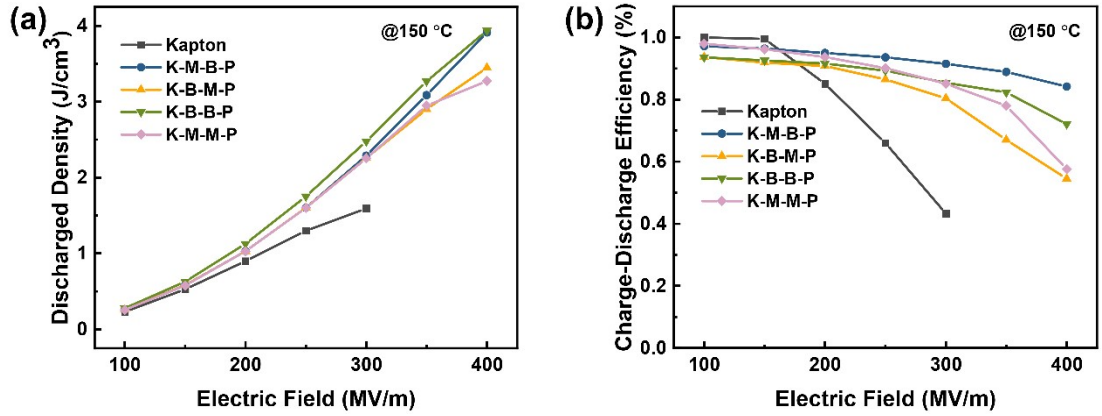

Fig. S23. (a) U_e and (b) η of Kapton PI and its bilayer nanocoated films measured at 150 °C.

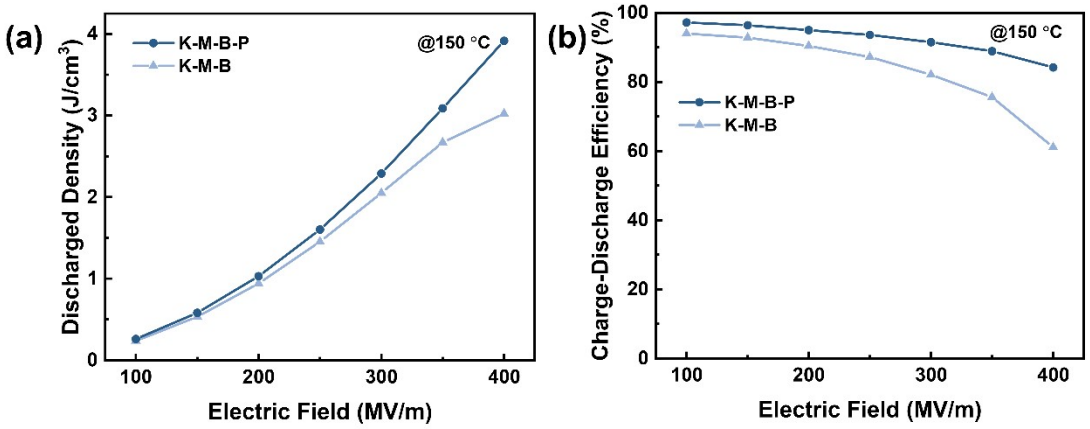

Fig. S24. (a) U_e and (b) η of K–M–B and K–M–B–P samples measured at 150 °C.

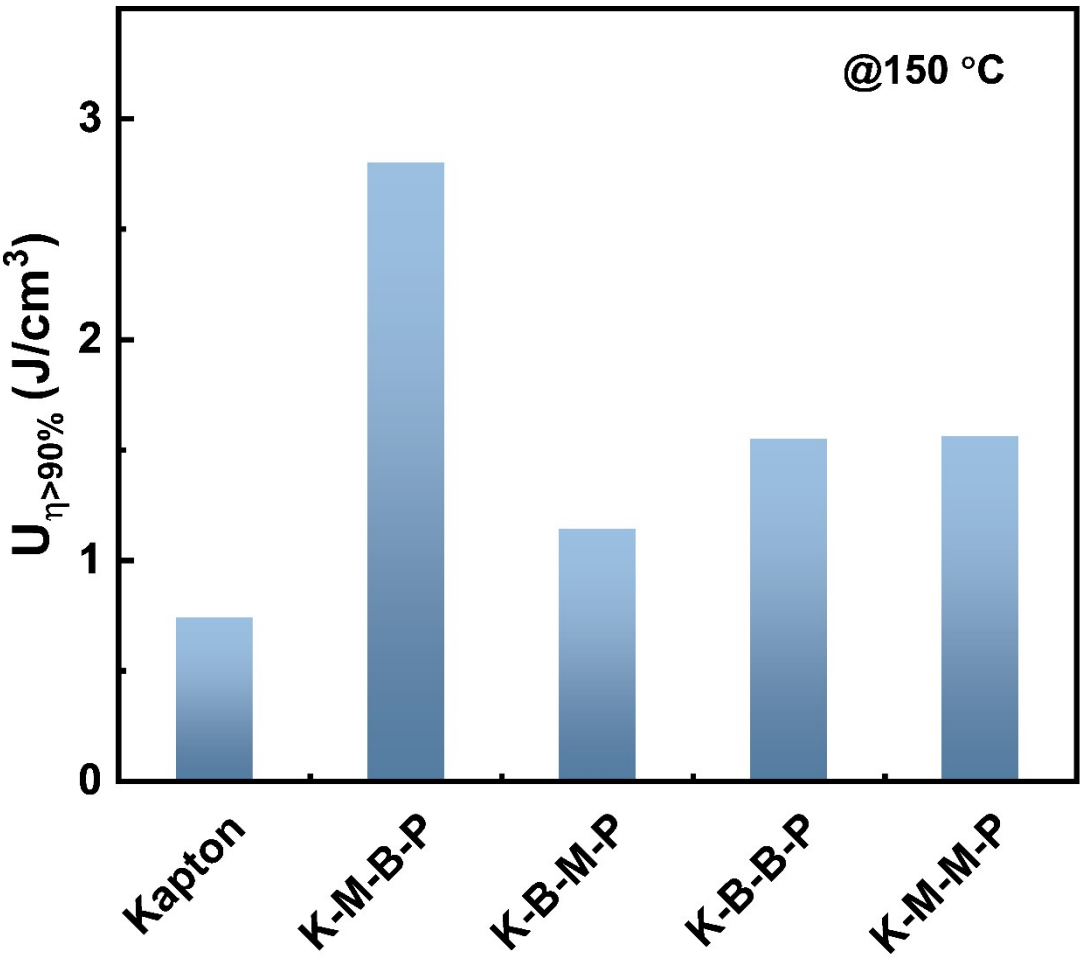

Fig. S25. U_e of various bilayer nanocoated Kapton PI films measured at 150 °C with η above 90%.

At 150 °C, although the K–B–B–P sample exhibits a relatively high U_e, its η is only 72.1% under an electric field of 400 MV m^{-1}. In contrast, the K–M–B–P sample achieves the highest η (84.2%) at the same field strength while maintaining a comparable high U_e (Fig. S21), significantly outperforming the K–M–M–P (57.6%) and K–B–M–P (54.5%) samples. A comparison between the K–M–B and K–M–B–P samples (Fig. S22) reveals that plasma treatment increases U_e from 3.02 to 3.91 J cm^{-3} and η from 61.1% to 84.2%. These results demonstrate that plasma treatment synergistically enhances both U_e and η.

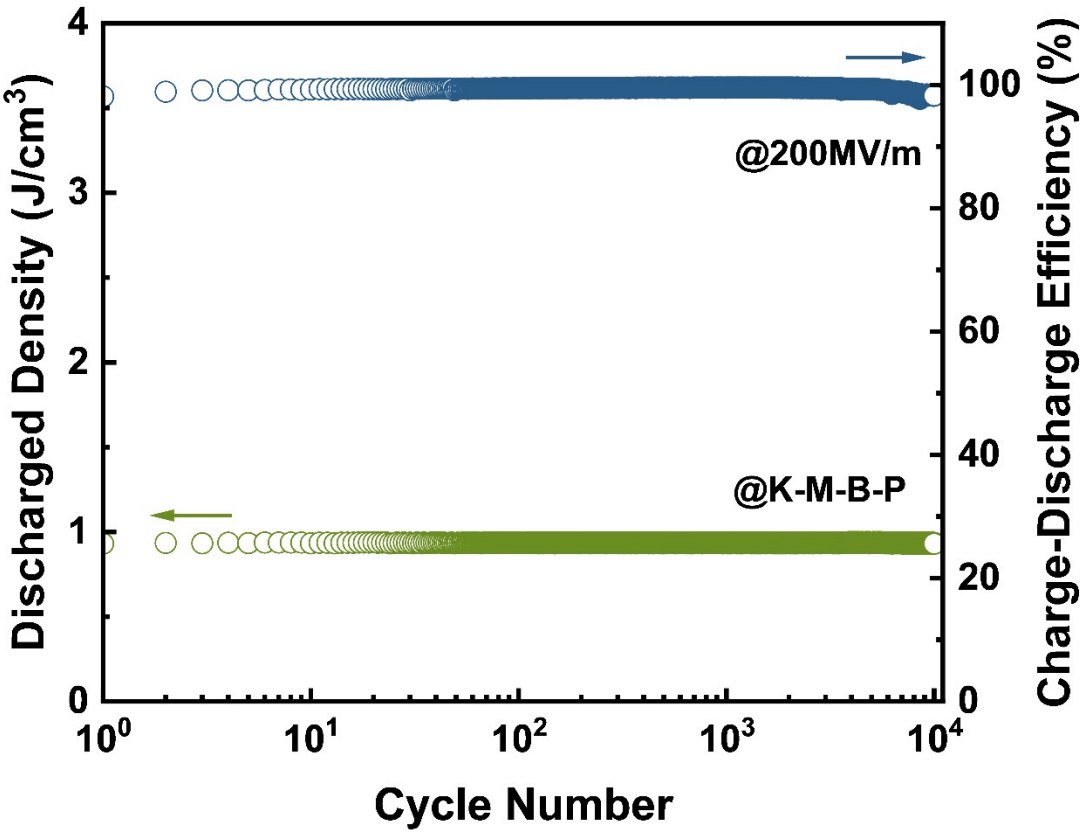

Fig. S26. Room-temperature U_e and η of the K–M–B–P sample as a function of cycle number at 200 MV m^{-1}.

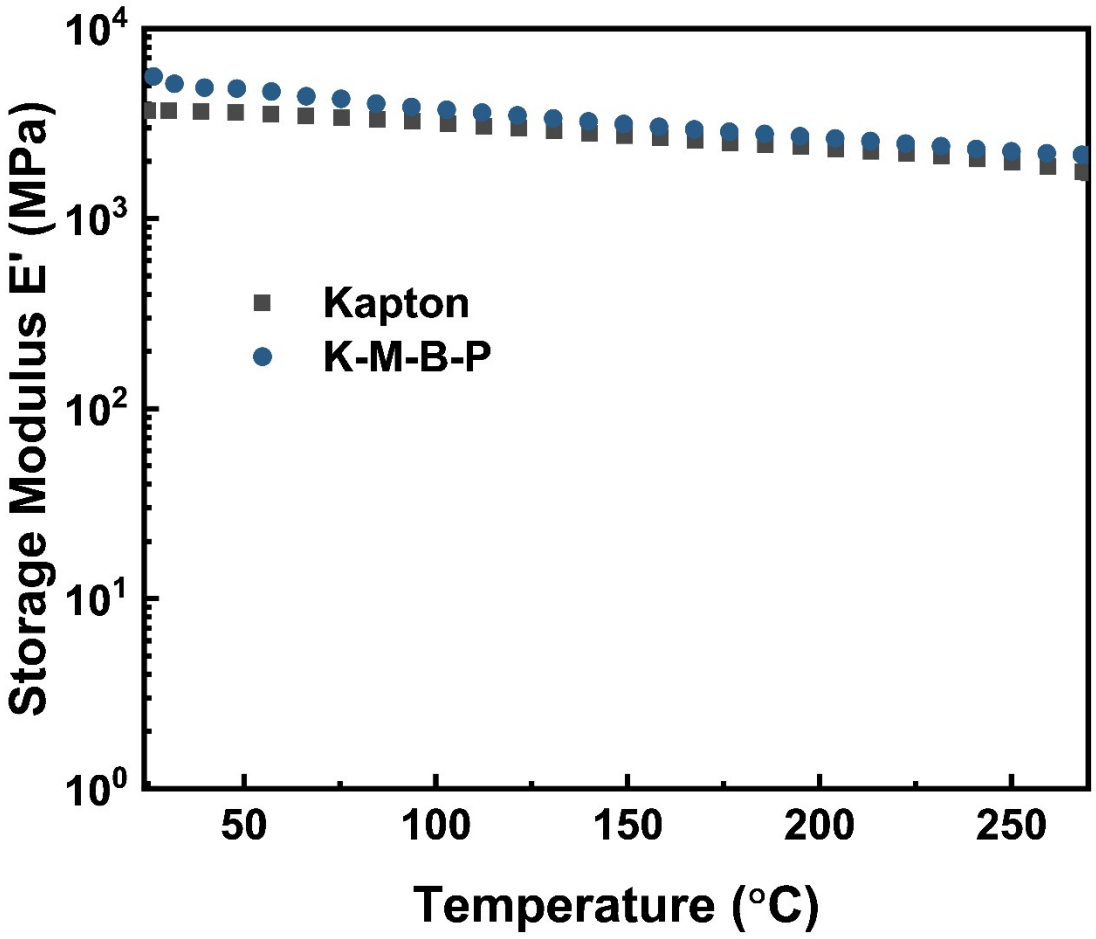

Fig. S27. Temperature-dependent storage modulus of K–M–B–P and pristine Kapton PI films measured via DMA.

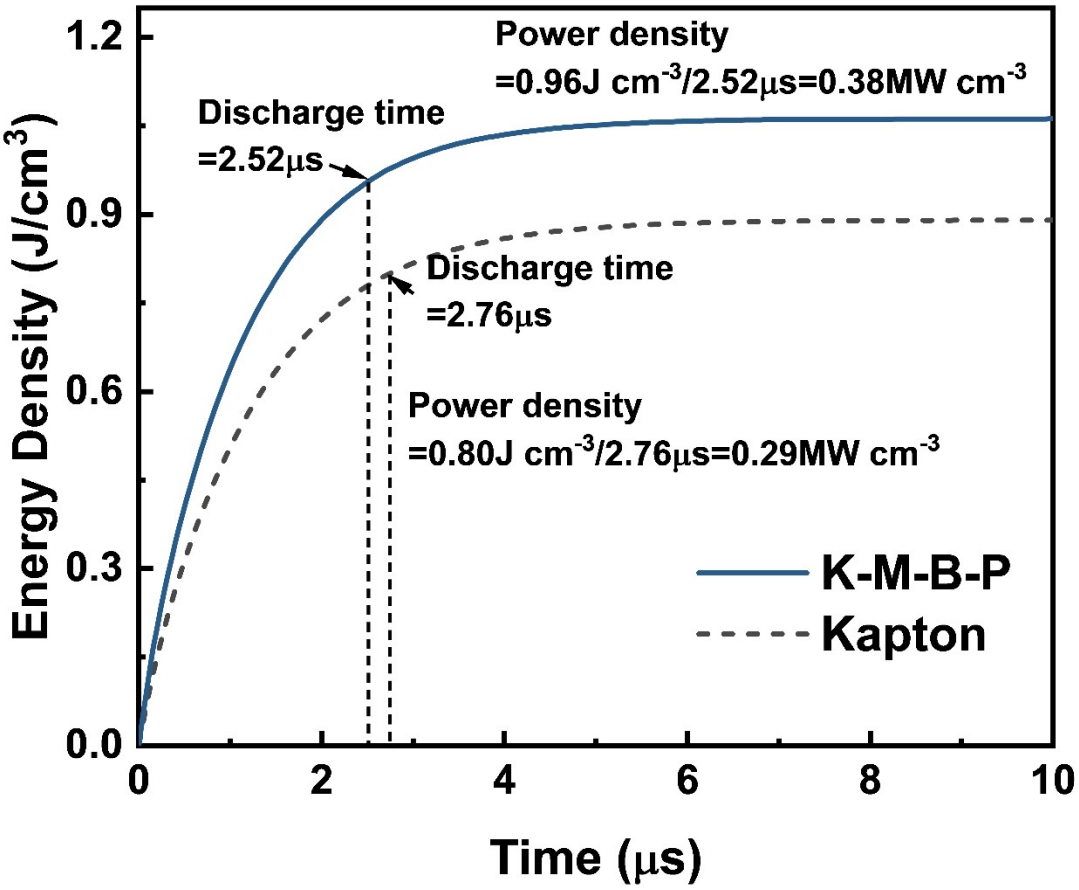

Fig. S28. Discharged energy density as a function of time for K–M–B–P and Kapton PI films, measured at 200 MV m^{-1} with a 10 kΩ load resistance at room temperature.